RESEARCH ARTICLE | JULY 01 1999

Particle acceleration in relativistic laser channels

A. Pukhov; Z.-M. Sheng; J. Meyer-ter-Vehn

Physics of Plasmas 6, 2847–2854 (1999)
https://doi.org/10.1063/1.873242

Particle acceleration in relativistic laser channels

A. Pukhov,[a] Z.-M. Sheng, and J. Meyer-ter-Vehn
Max-Planck-Institut für Quantenoptik, Hans-Kopfermann-Str. 1, 85748 Garching, Germany

(Received 4 January 1999; accepted 1 April 1999)

Energy spectra of ions and fast electrons accelerated by a channeling laser pulse in near-critical plasma are studied using three-dimensional (3D) Particle-In-Cell simulations. The realistic 3D geometry of the simulations allows us to obtain not only the shape of the spectra, but also the absolute numbers of accelerated particles. It is shown that ions are accelerated by a collisionless radial expansion of the channel and have nonthermal energy spectra. The electron energy spectra instead are Boltzmann-like. The effective temperature $T_{\rm eff}$ scales as $I^{1/2}$. The form of electron spectra and $T_{\rm eff}$ depends also on the length of the plasma channel. The major mechanism of electron acceleration in relativistic channels is identified. Electrons make transverse betatron oscillations in the self-generated static electric and magnetic fields. When the betatron frequency coincides with the laser frequency as witnessed by the relativistic electron, a resonance occurs, leading to an effective energy exchange between the laser and electron. This is the inverse free-electron laser mechanism. Electrons are accelerated at the betatron resonance when the laser power overcomes significantly the critical power for self-focusing. © *1999 American Institute of Physics.* [S1070-664X(99)02207-7]

I. INTRODUCTION

The Fast Ignition approach to inertial confinement fusion (ICF)[1] requires effective conversion of the Petawatt[2] laser power into hot electrons with given mean energy and angular spread.[1,3,4] This conversion takes place in nearly critical plasma where the laser pulse channels due to relativistic and ponderomotive effects.[5–9] Both experiments,[10–12] and Particle-in-Cell (PIC) simulations,[4,13] suggest that this conversion does operate with significant, up to 30%–40%, efficiency. In addition, PIC simulations clearly demonstrate that whenever a relativistically strong laser pulse channels or filaments in a near-critical plasma, strong currents of energetic, 10–100 MeV, electrons are generated.[8,14] These currents manifest themselves in a giant azimuthal quasistatic magnetic field with up to 100 MG amplitude.[15,16] The main mechanism of electron current generation by relativistically intense laser pulses still remains unclear. Single electron acceleration in vacuum by an intense focused laser beam has been studied previously (see, e.g., Ref. 17). Also, the influence of stochastic perturbations on single electron motion in an infinite plane electromagnetic wave has been discussed (see Ref. 18). Rigorous theoretical explanations for the form of hot electron spectra in near-critical plasma obtained experimentally or even numerically are still missing. The main reason for this situation is the intrinsically complex nature of the problem itself, as it involves many physical processes going on simultaneously.

In the present paper we undertake a systematic study of electron and ion acceleration in near-critical plasma by means of a three-dimensional (3D) PIC code VLPL (Virtual Laser Plasma Laboratory).[19] We show that the hot electron spectra have a Boltzmann-like form with an effective temperature $T_{\rm eff}$ which depends both on the laser pulse intensity and the channel or plasma scale length. The channel length is of high importance because it limits the distance over which the electrons can effectively gain energy from the laser pulse. Although intensity and channel length are the two decisive parameters, the form of the electron spectra may also depend on other pulse and plasma characteristics like laser pulse duration and temporal shape, target material, etc. In the present study, however, we abstract from these secondary dependencies.

We describe a new mechanism of direct laser energy coupling to hot plasma electrons. This coupling requires strong self-generated static electric and/or magnetic fields confining fast electrons in relativistic laser channels. An energetic electron experiences transverse betatron oscillations in the static fields. These oscillations are along the polarization of the laser pulse electric field, and thus an efficient energy exchange is possible when the betatron frequency is close to the laser frequency, as witnessed by the relativistic electron. The fast electrons are produced in resonant bunches at each half laser period. This kind of acceleration at the betatron resonance is actually an inverse process to the so-called Ion Channel Laser (ICL), an exotic type of free electron laser (FEL) proposed by D. Whittum.[20] A distinctive feature of ICL is the absence of any preformed spatially periodic wiggler. Electrons, instead, oscillate in the self-generated fields. It is different from the B-loop mechanism,[13] since electrons do not need to leave and re-enter the laser focus. Acceleration at the betatron resonance works even for a plane electromagnetic wave, provided the static electric or magnetic fields are present.

The electrostatic field generated in the relativistic channel has the pinching polarity for electrons. The same electrostatic field pulls positively charged ions out of the channel

[a]Permanent address: Moscow Institute for Physics and Technology, Dolgoprudnyi, Moscow Region, Russia.

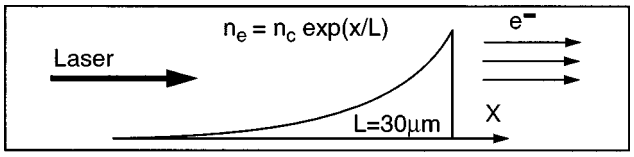

FIG. 1. Configuration used in the 3D PIC simulations. The laser pulse is incident on plasma with a density profile described by the exponent function. Energies of electrons reaching the right boundary are registered.

and accelerates them to MeV energies.[4,8,21,22] If the plasma ions are deuterons, fusion reactions are possible. These fusion reactions have been detected experimentally as neutron emission at the characteristic energy 2.45 MeV.[23,24] Here we present ion energy spectra obtained in 3D VLPL simulations for different laser powers.

II. 3D VLPL NUMERICAL SIMULATIONS

In order to gain more insight into the process of particle acceleration in near-critical plasma, we have performed a set of 3D PIC simulations. The initial configuration we have used in the numerical simulations is shown in Fig. 1. The laser pulse irradiates the left boundary of the simulation box. It is incident on the plasma with an exponential density profile $n(x)=n_0\exp(-x/L_s)$, where L_s is the plasma scale length. The maximum plasma density is higher than the critical one for the particular laser intensity. We chose this configuration because it is easy to be set up experimentally. Such a plasma can be formed on a surface of a solid state body with a naturally present[2] or deliberately created[24,25] prepulse. This prepulse heats the surface in some hundred picoseconds before the main pulse arrives. The plasma expands in the surrounding free space. The resulting density profile around the critical surface may be approximated by an exponential function.

There is a small gap of 1λ width between the right end of the plasma region and the right boundary of the simulation box. We record energies of electrons reaching the right boundary. These electrons are removed from the simulation. The average quasineutrality of the system is ensured by electrons flowing in at the lateral boundaries, where an electron density constant in time and equal to the local background one is maintained.[4] The plasma is assumed to be fully ionized initially with an ion charge-to-mass ratio equal to that of deuterium. Thus, our results can be applied to many different materials which, when fully ionized, have a similar charge-to-mass ratio.

The laser pulse is Gaussian in space and time with dimensionless amplitude $a=eA/mc^2=a_0\exp(-t^2/\tau^2)\exp(-r^2/\sigma^2)$, where t is time, and $r=\sqrt{y^2+z^2}$ is the distance from the axis. The time duration is set to $\tau=150$ fs and the laser is assumed to be focused at the left boundary in a round focal spot with the radius $\sigma=6\lambda$. When this geometry is maintained, the maximum intensity of the laser pulse is defined by its power. For our parameters $I/I_{18}=1.76P$ (TW), where $I_{18}=10^{18}$ W/cm^2. The laser is linearly polarized in the z-direction.

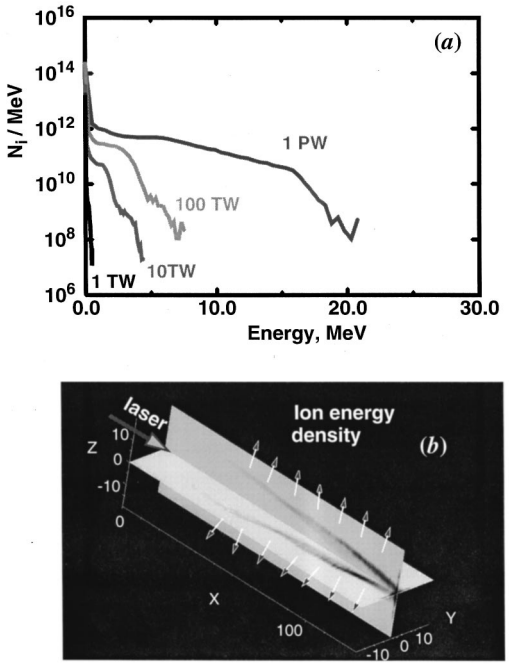

FIG. 2. (a) Ion energy spectra for different laser powers. The plasma scale length $L=30$ μm. (b) Ion energy density, perspective view. The white arrows indicate the channel expansion direction.

The simulations have been performed at Rechenzentrum Garching on a massively parallel computer CRAY-T3E with 784 processor elements.

A. Ion energy spectra

In the first series of numerical experiments we kept the plasma scale length $L_s=30\lambda$ fixed. We varied the laser peak intensity, and thus the power. The deuteron energy spectra obtained in the simulations with four different laser powers, 1 TW, 10 TW, 100 TW and 1 PW, are shown in Fig. 2(a). While the bulk of the ions in the simulation domain remains cold, a group of energetic ions appears. They have a relatively flat energy distribution up to some cutoff $E_i^{\max}$. These ions have been accelerated by radial expansion of the channel. A perspective view of the expanding channel for the Petawatt case is given in Fig. 2(b). It shows two longitudinal, $(X-Y)$ and $(X-Z)$, cuts of the ion energy density. The gray regions on the cuts correspond to the high energy density and mark the radially outgoing collisionless shock wave. The white arrows schematically show the direction of the channel expansion.

When the laser pulse channels due to the relativistic and charge-displacement effects, its radius collapses down to $R_{sf}\sim\gamma^{1/2}c/\omega_p$,[7] where $\omega_p=\sqrt{4\pi ne^2/m}$ is the plasma frequency, and $\gamma=\sqrt{1+(p/mc)^2}$ is the average relativistic γ-factor of plasma electrons in the laser field. The ponderomotive force tends to expel electrons from the channel. The simplified hydrodynamic description of the electron fluid[6,7] predicts complete electron cavitation around the channel axis. Our[4] and other[26] PIC simulations show that, although the electron density in the channel is suppressed, the cavitation is incomplete. This is because of the strong heating of plasma electrons in the channel by the laser pulse. We may

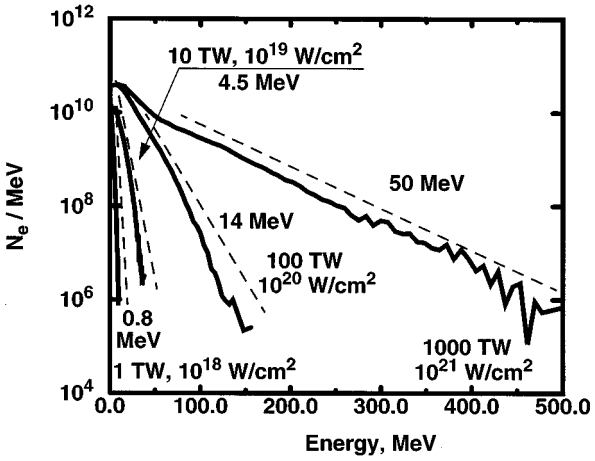

FIG. 3. Electron energy spectra for different laser powers. The plasma scale length $L=30$ μm.

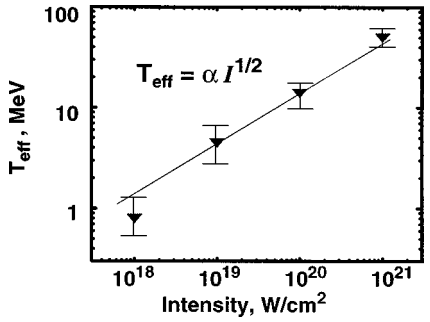

FIG. 4. Effective ''temperature'' of the electron distributions for different laser intensities. The best fit gives scaling $T_{\rm eff}\sim\alpha(I/I_{18})^{1/2}$, with $\alpha\approx 1.5$ MeV.

introduce the effective charge neutralization factor $f=n_e/n_i$ in the channel. Typically, $f\sim 0.5$.[9] The charge separation generates an electrostatic potential in the channel $e\phi_{ch}/mc^2\sim f(k_pR_{sf})^2$, where $k_p=\omega_p/c$. The subsequent Coulomb explosion of the channel accelerates the ions to energies defined by this potential. Assuming that the average γ-factor of the electrons in the channel scales like $\gamma\sim a_0$, we can estimate

$$E_i^{\max}\sim a_0mc^2\approx a_0\cdot 0.5\ \ \text{MeV}, \tag{1}$$

where estimation (1) agrees with the ion spectra in Fig. 2.

During the laser pulse passage time τ the channel expands to the radius $R_{\rm exp}=\tau\sqrt{2E_i^{\max}/M_i}$, raking up the surrounding plasma in a cylinder $R_{\rm exp}^2\times L_s$. Due to induced transparency,[4,27,28] a short ultrarelativistic laser pulse propagates freely up to the electron density $n\sim a_0n_c$, where n_c is the critical density. Consequently, we estimate the total number of accelerated ions as

$$N_i\sim\pi n_iR_{\rm exp}^2L_s=2\pi a_0^2n_c(c\tau)^2L_s\frac{m}{ZM_i}, \tag{2}$$

where Z is the ion charge state.

The estimation (2) is valid if during the laser pulse passing time the channel expands to a radius $R_{\rm exp}$ smaller than the vacuum focal spot σ of the laser. Otherwise we may substitute σ for $R_{\rm exp}$ in (2).

B. Electron spectra

Figure 3 shows spectra of fast electrons obtained at four different laser powers: 1 TW, 10 TW, 100 TW and 1 PW. The spectra indicate an approximately exponential roll-off at high energies,

$$n_e(\varepsilon)\sim n_0\exp(-\varepsilon/T_{\rm eff}), \tag{3}$$

with an ''effective temperature'' $T_{\rm eff}$ growing with the laser intensity. Figure 4 illustrates the dependence of $T_{\rm eff}$ vs laser intensity I in a logarithmic plot. The results of the numerical simulations suggest that $T_{\rm eff}$ grows like the square root of the intensity,

$$T_{\rm eff}\sim\alpha(I/I_{18})^{1/2}, \tag{4}$$

where the coefficient is $\alpha\approx 1.5$ MeV. The ''effective temperature'' for the Petawatt laser pulse appears to be as high as 50 MeV with the tail touching 0.5 GeV value. The density of electron energy distribution shows as much as 10^6 particles per MeV at this highest energy. Although we have approximated the energy spectra by the form (3), the exponential scaling fails at even higher energies. The cutoff energy is set by the finite force acting on the particle and the finite acceleration length. In our present simulations, however, we may not have resolved this cutoff because the number of macroparticles, although huge, up to 10^9, may be still too low. Each numerical macroparticle substitutes for about 10^5 physical electrons.

The scaling of the effective temperature $T_{\rm eff}$ with laser intensity like $\sim I^{1/2}$ coincides with the results of 2D PIC simulations,[3] in which a laser pulse interacted with a *sharply ramped* plasma-vacuum interface, and the electron heating mechanism is different.[29,30] However, the proportionality factor α obtained in the 3D simulations with a smooth ramp is significantly higher than that in Ref. 3. This higher effective temperature cannot be explained only by the intensity increase during the 3D self-focusing process.[8] Instead, it requires deeper insight into the mechanism of electron acceleration.

In order to investigate further the dependence of $T_{\rm eff}$ on plasma parameters, we have performed another series of simulations where we have varied the plasma scale length L_s from 3 to 50 μm. The length L_s limits the maximum channel length, and thus the acceleration distance. The laser pulse has the same parameters as defined above and a fixed power of 10 TW. Spectra of fast electrons are shown in Fig. 5. For the simulation with $L_s=3$ μm, i.e., for a relatively sharp density ramp, the electron spectrum has an exponential decay and the obtained $T_{\rm eff}$ is fairly close to the estimation of Ref. 3. As the plasma scale increases, however, the effective temperature grows. It is worthwhile to mention that for intermediate plasma scale lengths, $L_s=15$, 30 μm, the quasithermal distribution holds only up to some upper energy, and then falls sharper. This cutoff energy increases with the channel length, because the electrons can be accelerated on a longer distance. For $L_s=50$ μm the quasiexponential form of the spectrum extends to the resolution limit.

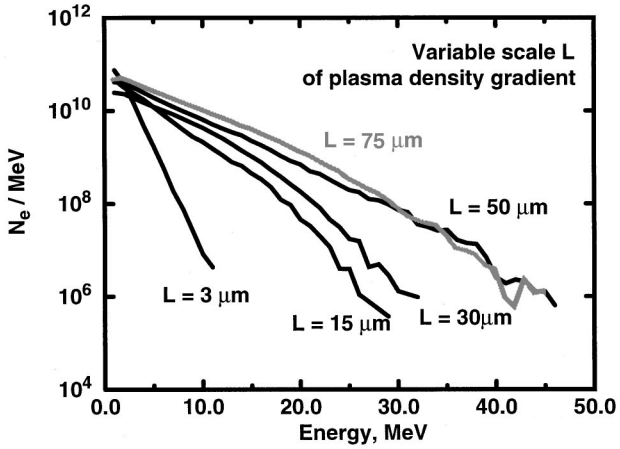

FIG. 5. Electron energy spectra for different plasma scale lengths. The laser power is 10 TW.

We find up to 90% absorption of the laser pulse energy in the plasma. However, the beam electron spectra presented in Figs. 3 and 5 contain only about 1% of the laser energy. This is significantly below the 30%–40% conversion into beam electrons obtained in 2D PIC simulations.[3,4] The difference is due to our measurement conditions. In Ref. 4 we have measured the energy transport by fast electrons *inside* the plasma, while in the present paper we count only those electrons that have left the plasma and touch the right boundary of the simulation domain. These electrons have to surmount the electrostatic potential ϕ_s building up at the right plasma boundary. The value of this potential may vary strongly depending on target material, size of the preformed plasma region, number of accelerated electrons, etc. This static potential diminishes the total number of fast electrons leaving the plasma. If we suppose that the fast electrons have a Boltzmann-like distribution (3) also inside the channel: $n_e = n_{ch} \exp(-\varepsilon/T_{\text{eff}})$, then we have $n_0 = n_{ch} \exp(-\phi_s/T_{\text{eff}})$. While the form of the spectrum is not influenced by the static potential, the number of electrons escaping the plasma decreases.

III. TEST 2D SIMULATION

The 3D PIC simulations display very rich and complicated physics of the laser-plasma interaction. Because of this complexity, some of the basic mechanisms of electron acceleration in relativistic channels are easier to analyze in 2D geometry. We have performed test PIC simulations with the 2D version of the code VLPL. A laser pulse with peak intensity of $I_0 = 10^{19}$ W/cm^2 and a transverse Gaussian profile with $\sigma = 2\lambda$ is incident on a 100λ thick slab of underdense plasma, $n_e = 0.16 n_c$. Ions in the plasma are kept immobile to prevent channel expansion which would complicate evaluation of the results. The laser is polarized in the y-direction (p-polarization). We have chosen the laser pulse to be rather narrow initially so that the laser pulse cannot focus further and change its intensity. Simulation results after 200 laser periods are presented in Fig. 6. Figures 6(a)–6(d) show distributions of (a) electron density n_e/n_c; (b) intensity I/I_{18}; (c) self-generated magnetic field B_z/B_0, where B_0

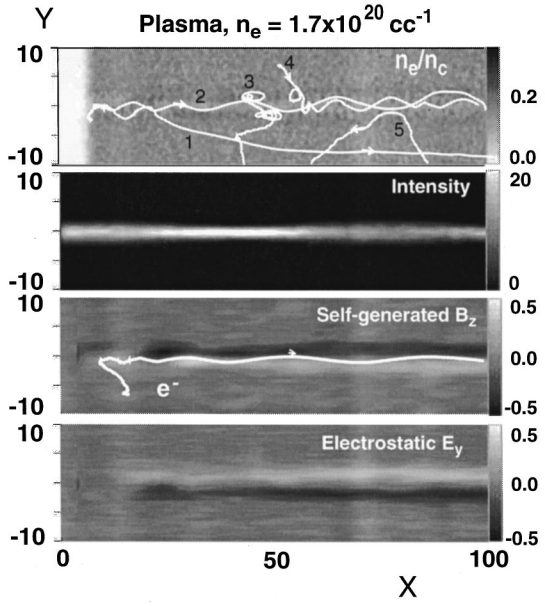

FIG. 6. Test 2D PIC simulations of laser, $I = 10^{19}$ W/cm^2, channeling in underdense, $n = 0.16 n_c$, plasma. (a) Electron density n_e/n_c; (b) intensity I/I_{18}; (c) self-generated magnetic field $eB_z/mc\omega_0$; (d) static electric field $eE_y/mc\omega_0$. The black numbers mark white lines corresponding to trajectories of individual electrons. For more detail see the text.

$= mc\omega_0/e = 107$ MG for a laser beam with 1 μm wavelength; (d) static electric field $eE_y/mc\omega_0$ in the channel. In addition, we have drawn trajectories of some selected electrons in Fig. 6(a). These trajectories represent different groups of electrons marked by the black numbers.

Electrons with numbers ''1,'' ''2,'' and ''4'' make betatron oscillations in the self-generated magnetic and electrostatic fields of the channel. The electron number ''1'' enters the channel at the mouth, while the number ''4'' penetrates through the channel wall. The electron number ''2'' has been scattered out of the channel after just a couple of betatron oscillations. The electron number ''3'' experiences cyclotron rotation in the quasistatic magnetic field at the channel boundaries. The electron number ''5'' contributes to the return current flowing around the channel. This electron drifts from outside toward the channel wall, bounces, and is scattered away by the static magnetic field, which has the defocusing polarity for the return current.

We have drawn separately the trajectory of the most energetic electron as the white line in Fig. 6(c). The electron originates in the background plasma outside of the channel. It slowly drifts to the channel mouth, catches the laser pulse at the right phase, and starts to gain energy continuously, making betatron oscillations in the channel. The trajectory in the longitudinal phase space of the electron is plotted in Fig. 7. The frequency of the betatron oscillations seen in the p_y plot slowly decreases as the electron is accelerated in the forward direction (see p_x plot). In addition to the secular acceleration, the p_x dynamics shows also oscillations at two times the betatron frequency. In our simulations we do not find any regular plasma wave, thus the only possible explanation for the electron energy gain is direct acceleration by the laser pulse. We also observe that oscillations of trans-

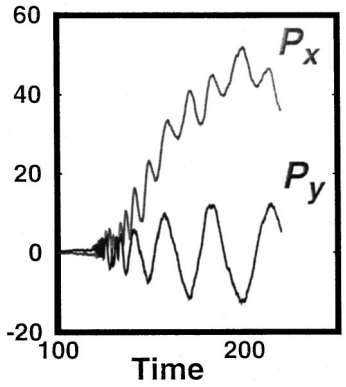

FIG. 7. Phase space of the fastest electron in the 2D PIC simulation. The transverse momentum, P_y, shows regular betatron oscillations of the electron in the self-generated fields. The longitudinal momentum, P_x, grows on average while displaying oscillations at *two times* the betatron frequency.

verse momentum of the electron have five times larger amplitude than that of the dimensionless laser vector potential. This shows clearly that the transverse motion of the electron is essentially oscillations in the channel potential well, driven resonantly by the laser field.

Other strong evidence for the mechanism of betatron resonance acceleration we find looking at the electron density inside the channel in Fig. 8. We observe an electron density modulation with two times per laser wavelength and a contrast $K=(n_{\max}-n_{\min})/(n_{\max}+n_{\min})\approx 0.3$. These modulations are similar to the natural microbunching of the fast electrons in inverse free electron lasers, as it has been experimentally observed (see, e.g., Ref. 31). The difference here is that in a usual FEL, electrons are bunched once per wavelength of the electromagnetic wave. This is because the electron motion is primarily governed by the wiggler. The resonant electrons have a fixed phase shift between the laser field and oscillations in the wiggler field.[32] As the wiggler phase is fixed in the space, the resonance can be achieved only once per laser wavelength. The situation is different in the plasma channel. The phase of betatron oscillations is not fixed spatially, and, when in resonance, is attached to the laser phase only. As we are considering a linearly polarized laser beam, the transverse velocity of the resonant electrons $\beta_\perp = v_\perp/c$ oscillates with the laser period, while the longitudinal velocity $\beta_\parallel \approx 1-\beta_\perp^2/2$ oscillates twice per laser period, leading to the electron bunching in space two times per laser wavelength. In simulations with a circularly polarized laser beam, such bunching is naturally absent.

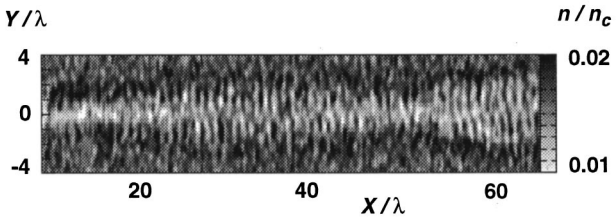

FIG. 8. Electron density inside channel. Electron bunching at half the laser wavelength is seen.

IV. ELECTRON ACCELERATION AT BETATRON RESONANCE

The presence of self-generated fields is the characteristic feature of a laser pulse channeling in plasma due to relativistic and ponderomotive effects. Ponderomotive expulsion of background plasma electrons from the channel creates a radial electrostatic field, while the current of the accelerated electrons generates an azimuthal magnetic field. Both these fields depend about linearly on radius and reach their maxima at the channel boundaries. We have to take into account the influence of these fields on the electron dynamics to understand the mechanism of acceleration. Such an acceleration in the presence of a self-generated magnetic field has been already considered in Ref. 13, where we called it B-loop mechanism. In the present paper we generalize our consideration by taking into account the electrostatic field and giving more insight into the details of the acceleration.

Let us consider an electron moving in a plane electromagnetic wave $E_y^l = E_0 \cos\omega_0(t-x/v_{ph})$, $B_z = E_y/v_{ph}$, which runs with the phase velocity $v_{ph}>c$ in the X-direction. In addition, we impose a static electric field $E_y^s=\kappa_E y$ and a magnetic field $B_z^s=-\kappa_B y$. For simplicity, we exploit planar 2D (X-Y) geometry. In the following discussion, we will use the dimensionless variables

$$p\to p/mc; \quad v\to v/c; \quad t\to \omega_0 t;$$
$$x\to x\omega_0/c; \quad E\to eE/m\omega_0 c; \quad B\to eB/m\omega_0. \tag{5}$$

In these variables, one can write down the equations of particle motion

$$\frac{dp_x}{dt} = -\frac{v_y}{v_{ph}}E^l - v_y B^s, \tag{6}$$

$$\frac{dp_y}{dt} = -\left(1-\frac{v_x}{v_{ph}}\right)E^l - E^s + v_x B^s, \tag{7}$$

$$\frac{d\gamma}{dt} = -v_y(E^l+E^s). \tag{8}$$

Using the expressions $B^s=-\kappa_B y$ and $E^s=\kappa_E y$ for the static fields, we can immediately find from Eqs. (6) and (8) the constant of motion

$$-v_{ph}p_x + W = W_0, \tag{9}$$

where

$$W=\gamma-1+(\kappa_E+v_{ph}\kappa_B)y^2/2 \tag{10}$$

is the sum of the kinetic $K=\gamma-1$ and the potential $U=(\kappa_E+v_{ph}\kappa_B)y^2/2$ energy of the particle in the static fields. Here $\gamma=\sqrt{1+p_x^2+p_y^2}$ is the relativistic γ-factor.

An exact analytical solution of Eqs. (6)–(8) is impossible because of their nonlinearity. Nevertheless, these equations reveal the mechanism of acceleration. To make it explicit, we rewrite the equation for transverse motion (7) as

$$\frac{d^2y}{dt^2}+\omega_\beta^2 y = \left[\left(\frac{dy}{dt}\right)^2 - \left(1-\frac{v_x}{v_{ph}}\right)\right]\frac{E^l}{\gamma} + \left(\frac{dy}{dt}\right)^2\frac{\kappa_E y}{\gamma}. \tag{11}$$

This is indeed an equation of a driven oscillator with the eigenfrequency

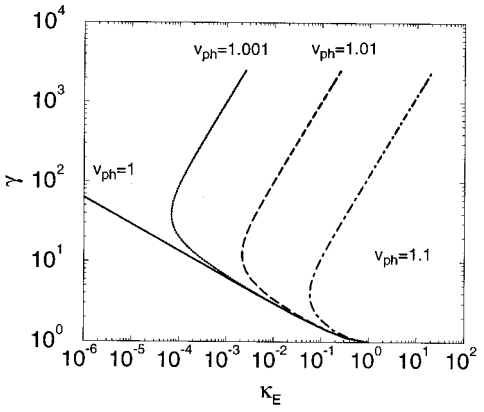

FIG. 9. Dependence of the resonant electron energy γ on the electrostatic field parameter κ_E for different phase velocities of the electromagnetic wave. For $v_{ph}>1$, the self-generated fields must be sufficiently strong for the resonance to appear.

$$\omega_\beta^2=(\kappa_E+v_x\kappa_B)/\gamma, \tag{12}$$

corresponding to betatron oscillations in the static E^s and B^s fields. The driving force on the right-hand side (RHS) of Eq. (11) hits the resonance when

$$\omega_\beta=1-v_x/v_{ph}. \tag{13}$$

This resonance condition states that when an electron makes one oscillation, the electromagnetic wave, which propagates with $v_{ph}>c$, overtakes it exactly by one period. It appears that, for the general case $v_{ph}>1$, the resonant electron energy γ is not a monotonical function of κ_E and κ_B. This is shown in Fig. 9, where we have set $\kappa_B=0$ for simplicity. In particular, for a given $v_{ph}>1$, the resonance can only be achieved for a sufficiently strong self-generated electrostatic field satisfying the condition $\kappa_E>\gamma_0[5v_{ph}^2+4-3v_{ph}(v_{ph}^2+8)^{1/2}]/(2v_{ph}^2)$, where the resonant energy $\gamma_0=\sqrt{2}[v_{ph}(v_{ph}^2+8)^{1/2}-v_{ph}^2-2]^{-1/2}$ (or $v_x=[-v_{ph}+(v_{ph}^2+8)^{1/2}]/2$). For very strong self-generated fields, i.e., higher parameters κ_E, the resonance can be achieved at two different energies, as seen in Fig. 9.

The physics relevant here is very similar to that of inverse free electron lasers.[33] However, instead of being bent by a periodic wiggler, electrons make betatron oscillations in the self-generated fields. Equations describing the inverse free electron laser at the betatron resonance (β-IFEL) strongly simplify in the ultrarelativistic limit $\gamma\gg1$. Then, ω_β changes slowly on the time scale of one betatron oscillation and for the transverse electron motion we may write

$$p_y=P_y\cos\theta_\beta, \quad d_t\theta_\beta=\omega_\beta, \tag{14}$$

where P_y is the magnitude of the oscillating transverse momentum. The maximum transverse displacement of the electron is $y_0=P_y/\omega_\beta$. The laser electric field at the electron position is $E^l=E_0\cos(t-x/v_{ph})$. Using (8) we write down the final set of β-IFEL equations,

$$d_x\left(\gamma+\frac{\kappa_E y^2}{2}\right)=-E_0\frac{P_y}{2p_x}(\cos\Psi+\cos\psi), \tag{15}$$

$$v_x d_x\Psi=\omega_\beta-\left(1-\frac{v_x}{v_{ph}}\right), \tag{16}$$

$$v_x d_x\psi=\omega_\beta+\left(1-\frac{v_x}{v_{ph}}\right), \tag{17}$$

where Ψ is the ponderomotive phase (slow oscillatory) of an electron in the bucket produced by the laser wave, while the fast phase ψ rotates as $2\omega_\beta t$. These oscillations at twice the betatron frequency are clearly seen in the p_x plot of Fig. 7.

As it follows from the gain, Eq. (15), electrons are accelerated if their ponderomotive phase satisfies $\pi/2<\Psi<3\pi/2$, and are decelerated otherwise. The maximum acceleration is achieved when the betatron oscillations are exactly in counterphase with the laser electric field (because of the negative electron charge). This means that when the electron moves with its highest transverse velocity at the channel axis, the electric field of the laser pulse is at its maximum and has the accelerating direction. When the electron reaches the turning point at the channel boundary, the laser field vanishes. As the electron reverses its transverse motion, the direction of the laser electric field reverses either, and the energy gain continues.

The continuous growth of γ leads to the corresponding ω_β decrease and detuning according to Eq. (16). The electron dephases and acceleration ceases. To describe this effect quantitatively we use Eqs. (15) and (16) and obtain for the ponderomotive phase Ψ the usual FEL nonlinear pendulum equation,[34]

$$d_t^2\Psi=E_0\frac{\omega_\beta}{4\gamma}\sin\alpha\cos\Psi. \tag{18}$$

Here, α is the average angle of electron propagation direction with respect to the channel axis, so that $\sin\alpha=P_y/\gamma$. We neglected smaller terms $\sim\gamma^{-3}$. After many synchrotron rotations in the bucket, the phase space is mixed. Also, different electrons run at different angles α to the channel axis, and the electron energy spectrum thermalizes. As we see from Eq. (15), the electron energy gain is proportional to the laser pulse electric field E_0, which in turn is $\sim I^{1/2}$. Thus, we expect the effective electron ''temperature''to depend on the laser intensity in the same way; an accurate derivation of the dependence is still pending.

Equation (18) tells us that the electrons are making synchrotron oscillations in the ponderomotive bucket with the bouncing frequency $\Omega_B=(E_0\omega_\beta\sin\alpha/4\gamma)^{1/2}$. The bucket height is $2\Omega_B$. Electrons are becoming trapped in the bucket if they enter it with $|d_t\Psi|<2\Omega_B$. At high laser intensities and strong static fields, the bucket is sufficiently deep to trap even low energy background electrons. One may estimate the threshold to be

$$E_0^2(\kappa_E+v_x\kappa_B)>1. \tag{19}$$

When the trapping condition (19) is not satisfied, the electrons can be preaccelerated by the plasma wakefield and then be trapped.

In the discussion above, we supposed the channel to be infinite in the transverse direction. This is not the case in reality. As the electrons are making transverse oscillations,

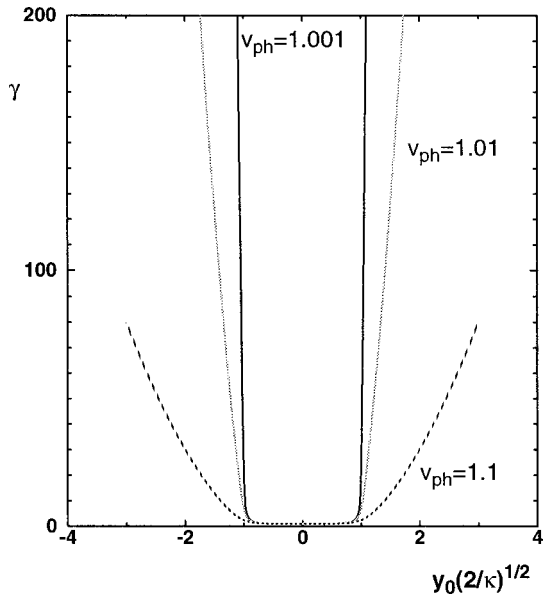

FIG. 10. Relativistic γ-factor of an electron vs transverse extent y_0 of betatron oscillations for different phase velocities v_{ph} of the laser pulse.

they may overtake the potential barrier and leave the channel transversely. Thus, the potential well associated with the channel must be sufficently deep and wide to trap the fast electrons. Some interesting estimations can be obtained from the conservation law (10). It connects the particle energy with its transverse position and the channel parameters. The expression is greatly simplified for an electron initially at rest at the channel axis, so that $W_0=0$. Furthermore, we can use the fact that the transverse momentum is $p_y=0$ at the maximum displacement from the axis, and obtain

$$\gamma=\gamma_{ph}^2\left[\frac{\kappa y_0^2}{2}-1+v_{ph}\sqrt{\gamma_{ph}^{-2}+\left(\frac{\kappa y_0^2}{2}-1\right)^2}\right], \tag{20}$$

where $\gamma_{ph}^2=1/(v_{ph}^2-1)$, and $\kappa=\kappa_E+v_{ph}\kappa_B$. Figure 10 shows how γ depends on the oscillation amplitude y_0. The behavior is thresholdlike. For small oscillations nearby the channel axis, the particle energy gain is small. As soon as the amplitude y_0 becomes larger than the critical radius $\rho_\beta=\sqrt{2/\kappa}$, the energy gain takes off steeply as $\gamma\sim\gamma_{ph}^2(1+v_{ph})\kappa y_0^2/2$. The closer the phase velocity v_{ph} is to the speed of light, the steeper is the dependence. This allows us to draw two conclusions. (i) The hot electrons oscillate in the channel within the radius ρ_β. (ii) The background plasma electrons are accelerated by the betatron resonance mechanism only if the self-generated fields in the channel are sufficiently strong,

$$\rho(E_{\max}+B_{\max})>2, \tag{21}$$

where $E_{\max}$ and $B_{\max}$ are the maximum static fields at the channel boundary at radius ρ.

The condition (21) can be expressed in terms of laser intensity or power. For simplicity, we neglect the magnetic field, and consider the electrostatic fields only. This assumption is valid at the beginning of the interaction, when the plasma is still cold and most of the background electrons are expelled from the channel due to the ponderomotive force. Balancing the electrostatic field with the ponderomotive force, we may estimate $E_{\max}\sim\sqrt{1+a_0^2/2}/\rho$, where a_0 is the laser amplitude at the axis and ρ is the radius of the laser filament. Substituting $E_{\max}$ in (21) we find the condition $a_0^2>2$ for the laser amplitude, or for the intensity $I\lambda^2>2.74\times10^{18}$ Wμm^2/cm^2. According to the results of Refs. 6 and 7, this condition is satisfied as soon as the laser power significantly exceeds the critical power for self-focusing,

$$P_c=17GW\cdot\frac{n_c}{n}, \tag{22}$$

and a cavitated region appears.

3D PIC simulations[13] do suggest that this mechanism of electron acceleration acts in relativistic channels in an underdense plasma when the laser power is significantly higher than P_c. The simulations suggest that the threshold power P_{th} is about $6P_c$.

V. DISCUSSION

In summary, we have shown by 3D Particle-In-Cell simulations with the code VLPL that electrons accelerated by laser pulses in relativistic channels have Boltzmann-like energy spectra. The effective temperature scales like $T_{\text{eff}}\sim1.5$ MeV $(I/I_{18})^{1/2}$. This temperature, however, seems to be a limit achieved when the plasma scale length is sufficiently long. For sharply edged overdense plasmas, the temperature scaling is lower, as described in Ref. 3. At intermediate density lengths the energy spectrum deviates from the Boltzmann form in the high energy tail.

We have identified the dominant mechanism of electron acceleration in relativistic channels. When the frequency of the transverse electron oscillations in the self-generated static electric and magnetic fields (betatron oscillations) coincides with the laser frequency as witnessed by the relativistic electron, a resonance occurs. The electron motion is along the laser pulse polarization, and an effective energy exchange between the laser and electron takes place. This is the inverse free electron laser at the betatron resonance. The acceleration at the betatron resonance effectively works when the laser power overcomes significantly the critical power for self-focusing. It is also one of the most effective mechanisms of laser energy absorption in relativistic channels, and is particularly important for the fast ignition of ICF targets.[1,4]

ACKNOWLEDGMENTS

The authors thank N. J. Fisch, G. Shvets, and M. Haines for fruitful discussions. This work was supported in part by Deutsche Forschungsgemeinschaft, Bundesministerium für Forschung und Technologie, by EURATOM, and by the Humboldt Foundation.

[1] M. Tabak, J. Hammer, M. E. Glinsky, W. L. Kruer, S. C. Wilks, J. Woodworth, E. M. Campbell, M. D. Perry, R. J. Mason, Phys. Plasmas **1**, 1626 (1994).
[2] G. Mourou, C. Barty, and M. D. Perry, Phys. Today **51**, 22 (1998).
[3] S. C. Wilks, W. L. Kruer, M. Tabak, and A. B. Langdon, Phys. Rev. Lett. **69**, 1383 (1992).

[4]A. Pukhov and J. Meyer-ter-Vehn, Phys. Rev. Lett. **79**, 2686 (1997).
[5]G. Schmidt and W. Horton, Comments Plasma Phys. Control. Fusion **9**, 85 (1985).
[6]G. Z. Sun, E. Ott, Y. C. Lee, and P. Guzdar, Phys. Fluids **30**, 526 (1987).
[7]A. B. Borisov, O. B. Shiryaev, A. McPherson, K. Boyer, and C. K. Rhodes, Plasma Phys. Controlled Fusion **37**, 569 (1995).
[8]A. Pukhov and J. Meyer-ter-Vehn, Phys. Rev. Lett. **76**, 3975 (1996).
[9]M. Borghesi, A. J. MacKinnon, L. Barringer, R. Gaillard, L. A. Gizzi, C. Meyer, O. Willi, A. Pukhov, and J. Meyer-ter-Vehn, Phys. Rev. Lett. **78**, 879 (1997).
[10]M. H. Key, M. D. Cable, T. E. Cowan *et al.*, Phys. Plasmas **5**, 1966 (1998).
[11]K. B. Wharton, C. Brown, B. A. Hammel, S. Hatchett, M. H. Key *et al.*, Phys. Rev. Lett. **81**, 822 (1998).
[12]G. Malka, J. Fuchs, F. Amiranoff, S. D. Baton, R. Gailard, J. L. Miquel, H. Pepin, C. Rousseaux, G. Bonnaud, M. Busquet, and L. Lours, Phys. Rev. Lett. **78**, 2053 (1997).
[13]A. Pukhov and J. Meyer-ter-Vehn, Phys. Plasmas **5**, 1880 (1998).
[14]G. A. Askar'an, S. V. Bulanov, F. Pegoraro, and A. Pukhov, JETP Lett. **76**, 3975 (1994).
[15]M. Borghesi, A. J. Mackinnon, R. Gaillard, O. Willi, A. Pukhov, and J. Meyer-ter-Vehn, Phys. Rev. Lett. **80**, 5137 (1998).
[16]J. Fuchs, G. Malka, J. C. Adam, F. Amiranoff *et al.*, Phys. Rev. Lett. **80**, 1658 (1998).
[17]B. Quesnel and P. Mora, Phys. Rev. E **58**, 3719 (1998).
[18]J. Meyer-ter-Vehn and Z. M. Sheng, Phys. Plasmas **6**, 641 (1999).
[19]A. Pukhov, J. Plasma Phys. (in press).
[20]D. H. Whittum, Phys. Fluids B **4**, 730 (1992).
[21]N. H. Burnett and G. D. Enright, IEEE J. Quantum Electron. **26**, 1797 (1990).
[22]G. S. Sarkisov, V. Yu. Bychenkov, A. V. Tikhonchuk, A. Maksimchuk *et al.*, JETP Lett. **66**, 828 (1997).
[23]P. Norreys, Plasma Phys. Controlled Fusion **40**, 175 (1998).
[24]G. Pretzler, A. Saemann, A. Pukhov, D. Rudolph *et al.*, Phys. Rev. E **58**, 1165 (1998).
[25]C. Gahn, G. Pretzler, A. Saemann, G. D. Tsakiris *et al.*, Appl. Phys. Lett. **73**, 3662 (1998).
[26]K.-C. Tzeng and W. B. Mori, Phys. Rev. Lett. **81**, 104 (1998).
[27]E. Lefebvre and G. Bonnaud, Phys. Rev. Lett. **74**, 2002 (1995).
[28]S. Guerin, P. Mora, J. C. Adam, A. Heron, and G. Laval, Phys. Plasmas **3**, 2693 (1996).
[29]F. Brunel, Phys. Rev. Lett. **59**, 52 (1987).
[30]H. Ruhl and P. Mulser, Phys. Lett. A **205**, 388 (1995).
[31]Y. Liu, X. J. Wang, D. B. Cline, M. Babzien *et al.*, Phys. Rev. Lett. **80**, 4418 (1998).
[32]T. Marshall, *Free Electron Lasers* (MacMillan, New York, 1985), p. 42.
[33]E. D. Courant, C. Pellegrini, and W. Zakowicz, Phys. Rev. A **32**, 2813 (1985).
[34]G. Dattoli, A. Renieri, and A. Torre, *Lectures on the Free Electron Lasers and Related Topics* (World Scietific, Singapore, 1993), pp. 289–342.